

Observation of Josephson effect in ^{23}Na spinor Bose-Einstein condensates

Yong Qin(秦永), Xin Wang(王鑫), Jun Jian(蹇君), Wenliang Liu(刘文良), Jizhou Wu(武寄洲), Yuqing Li(李玉清), Jie Ma(马杰), Liantuan Xiao(肖连团), and Suotang Jia(贾锁堂)

Citation: Chin. Phys. B, 2025, 34 (**3**): 033701. DOI: 10.1088/1674-1056/ada42f
Journal homepage: http://cpb.iphy.ac.cn; http://iopscience.iop.org/cpb

What follows is a list of articles you may be interested in

Superfluid to Mott-insulator transition in a one-dimensional optical lattice

Wenliang Liu(刘文良), Ningxuan Zheng(郑宁宣), Jun Jian(蹇君), Li Tian(田丽), Jizhou Wu(武寄洲), Yuqing Li(李玉清), Yongming Fu(付永明), Peng Li(李鹏), Vladimir Sovkov, Jie Ma(马杰), Liantuan Xiao(肖连团), and Suotang Jia(贾锁堂)

Chin. Phys. B, 2022, 31 (**7**): 073702. DOI: 10.1088/1674-1056/ac6579

Enhanced cold mercury atom production with two-dimensional magneto-optical trap

Ye Zhang(张晔), Qi-Xin Liu(刘琪鑫), Jian-Fang Sun(孙剑芳), Zhen Xu(徐震), and Yu-Zhu Wang(王育竹)

Chin. Phys. B, 2022, 31 (**7**): 073701. DOI: 10.1088/1674-1056/ac5397

Dynamical properties of ultracold Bose atomic gases in one-dimensional optical lattices created by two schemes

Jiang Zhu(朱江), Cheng-Ling Bian(边成玲), Hong-Chen Wang(王红晨)

Chin. Phys. B, 2019, 28 (**9**): 093701. DOI: 10.1088/1674-1056/ab3448

Strontium optical lattice clock at the National Time Service Center

Ye-Bing Wang(王叶兵), Mo-Juan Yin(尹默娟), Jie Ren(任洁), Qin-Fang Xu(徐琴芳), Ben-Quan Lu(卢本全), Jian-Xin Han(韩建新), Yang Guo(郭阳), Hong Chang(常宏)

Chin. Phys. B, 2018, 27 (**2**): 023701. DOI: 10.1088/1674-1056/27/2/023701

Development of adjustable permanent magnet Zeeman slowers for optical lattice clocks

Xiao-Hang Zhang(张晓航), Xin-Ye Xu(徐信业)

Chin. Phys. B, 2017, 26 (**5**): 053701. DOI: 10.1088/1674-1056/26/5/053701

Observation of Josephson effect in ^{23}Na spinor Bose–Einstein condensates

Yong Qin(秦永)[1], Xin Wang(王鑫)[1], Jun Jian(蹇君)[1], Wenliang Liu(刘文良)[1,2], Jizhou Wu(武寄洲)[1,2,†], Yuqing Li(李玉清)[1,2], Jie Ma(马杰)[1,2], Liantuan Xiao(肖连团)[1,2], and Suotang Jia(贾锁堂)[1,2]

[1] *State Key Laboratory of Quantum Optics and Quantum Optics Devices, Institute of Laser Spectroscopy, Shanxi University, Taiyuan* 030006, *China*
[2] *Collaborative Innovation Center of Extreme Optics, Shanxi University, Taiyuan* 030006, *China*

(Received 9 October 2024; revised manuscript received 27 December 2024; accepted manuscript online 31 December 2024)

The Josephson effect, an important quantum supercurrent phenomenon, has been extensively studied in superconductors and superfluids. In this paper, we investigate the rich physics of one-dimensional Josephson junctions in a red-detuned optical lattice with sodium (Na) quantum gas. A one-dimensional Josephson array is formed by setting up an optical lattice using a red-detuned laser. By characterizing the dependence of Josephson oscillations of the lattice depth, we experimentally demonstrate the Josephson current. The lattice depth is controlled by altering the lattice power, and our observations are consistent with theoretical predictions. These findings offer valuable insights into quantum coherent transport and the intricate dynamics inherent to superfluidity.

Keywords: Josephson junction, Josephson critical current, optical lattice, Bose–Einstein condensates

PACS: 37.10.Jk, 74.50.+r, 03.75.Lm

DOI: 10.1088/1674-1056/ada42f **CSTR:** 32038.14.CPB.ada42f

1. Introduction

The Josephson effect,[1] a macroscopic manifestation of quantum tunneling, characterizes the tunneling current through a Josephson junction composed of two weakly coupled superconductors.[2] Observations of the Josephson effect have been made across diverse experimental systems. Notably, in a superfluid helium system, quantum oscillations were observed when the dimensions of the aperture between two reservoirs were reduced to a size comparable to the healing length of the superfluid, thereby confirming the ideal Josephson effect.[3–5] Further exploration of the Josephson effect theory is anticipated to substantially advance the field of superconducting electronics and establish a solid foundation for quantum science applications, including quantum computing and quantum communications.[6,7]

Previous researches on the Josephson effect have mainly focused on superconducting or superfluid systems. Recently, there has been a surge of interests in the Josephson effect in ultracold atomic gas systems.[8,9] Initial investigations have concentrated on coupled Bose–Einstein condensates (BECs) in double-well traps[10,11] and coherently coupled spinor condensates.[12,13] In spin–orbit coupled BECs,[14] momentum-space Josephson junctions have been realized by coupling distinct momentum states via Raman-assisted tunneling. Additionally, Josephson oscillation between two weakly coupled fermionic superfluids[15] through an optical barrier has been observed. Josephson junction models have been constructed in weakly connected atomic condensates,[16,17] exhibiting both direct current (DC) and alternating current (AC) Josephson effects.[18] The simulation of a DC superconducting quantum interference device (SQUID)[19] has been achieved through the innovative implementation of a pair of toroidal Josephson junctions embedded within a diluted Bose–Einstein condensate. A variety of dynamical processes[20–22] have been explored, including the tunneling of atomic interactions[23] by manipulating the scattering length of atoms in a double-well trap using magnetic Feshbach resonance.[24–28] Within the theoretical framework of the two-dimensional (2D) Gross–Pitaevskii equation, a dynamic model for the long bosonic Josephson junction has been developed. The dynamic properties have been analyzed through a comprehensive examination of the excitation spectrum of the coupled condensates.[29]

The Josephson critical current represents the maximum current that a Josephson junction can sustain while maintaining a superconducting state with zero voltage. Critical current has been observed between two superfluid reservoirs in ultracold Fermionic systems,[30,31] where the sinusoidal current phase relationship characteristic of an ideal Josephson junction has been verified.[32,33] The Josephson critical current has been extensively studied in ultracold Fermionic systems. However, there are comparatively fewer reports on the Josephson critical current in Bosonic systems. Oscillating atomic currents have been observed in a ^{87}Rb Bose–Einstein condensate trapped in a blue-detuned periodic standing wave field.[34] Subsequently, a closed-loop atom circuit has been created and researched in a toroidal Bose–Einstein condensate.[35] But, none of these works addressed the Josephson effect in a red-detuned optical lattice.

[†]Corresponding author. E-mail: wujz@sxu.edu.cn

© 2025 Chinese Physical Society and IOP Publishing Ltd. All rights, including for text and data mining, AI training, and similar technologies, are reserved.

In this study, we construct a red-detuned one-dimensional (1D) optical lattice to explore the Josephson effect in an ultracold sodium bosonic gas. A ^{23}Na BEC is produced in the created 1D Josephson array. We probe the Josephson critical current by inducing tunneling oscillations of atoms between adjacent wells. Systematic measurements of the Josephson critical current are conducted as a function of the lattice depths. Our work has further enriched the study of Josephson effects in ultracold bosonic systems, such as coherent tunneling oscillations of interacting bosons and macroscopic quantum self-trapping phenomena.

2. Theoretical model

Josephson proposed in 1962[1] that supercurrents would emerge between two weakly coupled superconductors connected through a tunnel junction. At zero applied voltage, a quantum-mechanical phase difference of $\Delta\phi$ would induce a direct current. In the case of ideal superconductive tunneling, this current is given by[3]

$$J = J_0 \sin\Delta\phi, \tag{1}$$

where J_0 is the Josephson critical current. Furthermore, an electrochemical potential difference across the tunnel junction, denoted as ΔV, would result in the emergence of an alternating current. The frequency and magnitude of this current are determined by Eq. (1) with

$$\frac{\partial(\Delta\phi)}{\partial t} = -\frac{\Delta V}{\hbar}. \tag{2}$$

Properties of a BEC in a dilute gas can be adequately described within the mean-field approximation. The order parameter $\Psi(r,t)$ is introduced to characterize the condensate wavefunction, and it satisfies the Gross–Pitaevskii equation (GPE).[36] The effective Hamiltonian contains an extra nonlinear term $g|\Psi(r,t)|^2$, approximating an interatomic interaction (self-interaction) of the particles in the ultracold ensemble. Here $g = 4\pi\hbar^2 a/m$, m is the mass of a particle, a is the s-wave scattering length, $\hbar = h/2\pi$ is the Dirac constant, and $|\Psi(r,t)|^2 = n(r,t)$ is the local spatial density of the condensate. If the self-interaction is weak enough, the nonlinear term can be neglected, and the GPE becomes the standard Schrödinger equation. In many applications, it is convenient to present it in the form $\Psi(r,t) = \sqrt{n(r,t)}\exp(\mathrm{i}\phi(r,t))$.

The Josephson effect demonstrates the coherent behavior of an ultracold quantum ensemble through the tunneling phenomenon. It is observed when the entire ensemble is separated into many weakly coupled almost-stationary subsystems. The entire system can be described by a linear combination of the order parameters of those subsystems. Following Refs. [34,37], the wavefunction of the macroscopic phase of a quantum fluid is decomposed by a tight binding approximation

$$\Psi(r,t) = \sqrt{N_\mathrm{T}}\sum_k \psi_k(t)\varphi_k(r), \tag{3}$$

where N_T is the total number of the particles in the entire system, $\psi_k(t) = \sqrt{n_k(t)}\exp(\mathrm{i}\phi_k(t))$, $n_k(t) = N_k(t)/N_\mathrm{T}$, $N_k(t)$ is the number of particles within the k-th subsystem, $\varphi_k(r)$ is the stationary single-particle wavefunction within the k-th subsystem neglecting interactions with other subsystems.

We consider a 1D system, which can be realized via creating an elongated trap potential and a quasi-periodic extra potential oriented along the axis. Substituting Eq. (3) into the GPE, one obtains a system of coupled equations

$$\mathrm{i}\hbar\frac{\mathrm{d}\psi_k(t)}{\mathrm{d}t} = \left(\varepsilon_k + \Lambda|\psi_k|^2\right)\psi_k - K\psi_{k-1} - K\psi_{k+1}, \tag{4}$$

where the tunneling rate is proportional to the parameter

$$K \simeq -\int\left[\left(\hbar^2/2m\right)\nabla\varphi_k\cdot\nabla\varphi_{k+1} + \varphi_k V_\mathrm{ext}\varphi_{k+1}\right]\mathrm{d}\boldsymbol{r},$$

$$\varepsilon_k = \frac{1}{2K}\int\left[\frac{\hbar^2}{2m}\left(\nabla\varphi_k\right)^2 + V_\mathrm{ext}\varphi_k^2\right]\mathrm{d}\boldsymbol{r}, \quad \Lambda = \frac{g_0 N_\mathrm{T}}{2K}\int\varphi_k^4\,\mathrm{d}\boldsymbol{r}.$$

For the sake of simplicity, we consider a double-well system ($k = 1,2$) and neglect the self-interaction within each subsystem, i.e., assume $\Lambda = 0$. Additionally, we also introduce the designation $\lambda = (\varepsilon_2 - \varepsilon_1)/2$ and set the origin of the energy scale at the middle point between ε_1 and ε_2. This case the equations take the form of the ones, considered by Feynmann[38] in his very simple explanation of the Josephson effect

$$\mathrm{i}\hbar\frac{\mathrm{d}\psi_1(t)}{\mathrm{d}t} = -\lambda\,\psi_1 - K\psi_2, \tag{5a}$$

$$\mathrm{i}\hbar\frac{\mathrm{d}\psi_2(t)}{\mathrm{d}t} = \lambda\,\psi_2 - K\psi_1. \tag{5b}$$

After separating the real and imaginary parts, it results in a system comprised of four coupled first-order differential equations

$$\mathrm{i}\hbar\frac{\mathrm{d}n_k}{\mathrm{d}t} = (-1)^{k-1}K\sqrt{n_1 n_2}\sin\Delta\phi, \tag{6a}$$

$$\mathrm{i}\hbar\frac{\mathrm{d}\phi_k}{\mathrm{d}t} = -\frac{K}{\hbar}\left(\frac{n_1}{n_2}\right)^{k-3/2}\cos\Delta\phi + (-1)^k\frac{\lambda}{2\hbar}. \tag{6b}$$

Oscillations of a trapped ultracold ensemble can be excited by subjecting it to a jolt. In the absence of a lattice, supposing the trap potential to be the harmonic oscillator with frequency ω_0 along the elongated trap axis, the entire ensemble oscillates at this frequency ω_0, similar to the behavior of a pointlike particle. The superimposing of a lattice alternates this behavior. It is shown in Ref. [34] that such a behavior can be described in the collective coordinates $\xi = \sum_k k n_k$ (the weighted mean value of the well number) and $\Delta\phi = \phi_{k+1} - \phi_k$ (the phase difference between the order parameters of adjacent wells) by equations

$$\hbar\frac{\mathrm{d}\xi(t)}{\mathrm{d}t} = 2K\sin\Delta\phi(t), \tag{7a}$$

$$\hbar\frac{\mathrm{d}\Delta\phi(t)}{\mathrm{d}t} = -m\omega_0^2(\lambda/2)^2\xi(t), \tag{7b}$$

where λ is the wavelength of the lattice laser. These equations resemble typical pendulum-like equations. The notable feature of these equations is their independence from explicit interatomic interactions. From Eqs. (7a) and (7b), noting that the current is $J = N_t(\mathrm{d}\xi(t)/\mathrm{d}t)$, the critical Josepson current can be expressed as $J_0 = 2KN_\mathrm{T}/\hbar$. The parameter K depends on the height of the energy barrier V_0. By considering the oscillatory motion of atoms within the lattice structure and incorporating the concept of effective atomic mass[39,40] $m/m^* = (\omega/\omega_0)^2$, the value of m^* refers to states near the bottom of the energy band. Therefore, the critical current is given by

$$J_0 = \frac{4\hbar N_\mathrm{T}}{m\lambda^2}\left(\frac{\omega}{\omega_0}\right)^2, \tag{8}$$

where ω represents the actual frequency of the oscillations within the lattice. The dependencies predicted by this equation have been verified and confirmed through our experimental results.

3. Experimental setup

The experiment is conducted in a ^{23}Na BEC confined within a 1D optical lattice. The atomic beam from the oven chamber is decelerated by a Zeeman slower and captured in a conventional magneto–optical trap (MOT),[41] atom cloud is further cooled through a compressed magneto–optical trap (CMOT) and an optical molasses process.[42] Throughout the laser cooling stages (MOT, CMOT, and optical molasses), a crossed optical dipole trap (ODT), is maintained at a depth of 350 μK. The angle between the two beams (beam waist of 32 μm and 39 μm) is $\theta = 45°$. At the end of the laser cooling process, the ODT depth is increased to 700 μK. Following a 400-ms loading interval, approximately 2×10^6 atoms at 70 μK are confined within the ODT. Bose–Einstein condensate, containing 1.1×10^5 sodium atoms in the $F = 1$ state, is obtained by 2.5-s rapid evaporation cooling after the loading from the ODT. Detailed experimental procedures for the preparation of sodium BECs are provided in Ref. [43].

In this study, constructing the Josephson array is a critical step. A 1D optical lattice[44] is built to form the 1D Josephson array, as shown in Fig. 1(a). The optical lattice is generated using a red-detuned 1064-nm fiber laser (ALS-IR-1064, 30 W). The laser beam passes through an acousto–optic modulator (AOM), and the diffracted beam traverses atomic cloud before being reflected by a mirror. This configuration creates counter-propagating optical fields, resulting in an optical lattice ($1/e^2$ radius of ~ 39 μm) with a lattice constant of 532 nm. A pair of Helmholtz (anti-Helmholtz) coil, is used to create bias (gradient) magnetic field around the central position of the atoms. The quantized initial states are prepared by the coils. Atoms in the $|F = 1, m_F = -1\rangle$ state are loaded into the optical lattice to form the Josephson array.

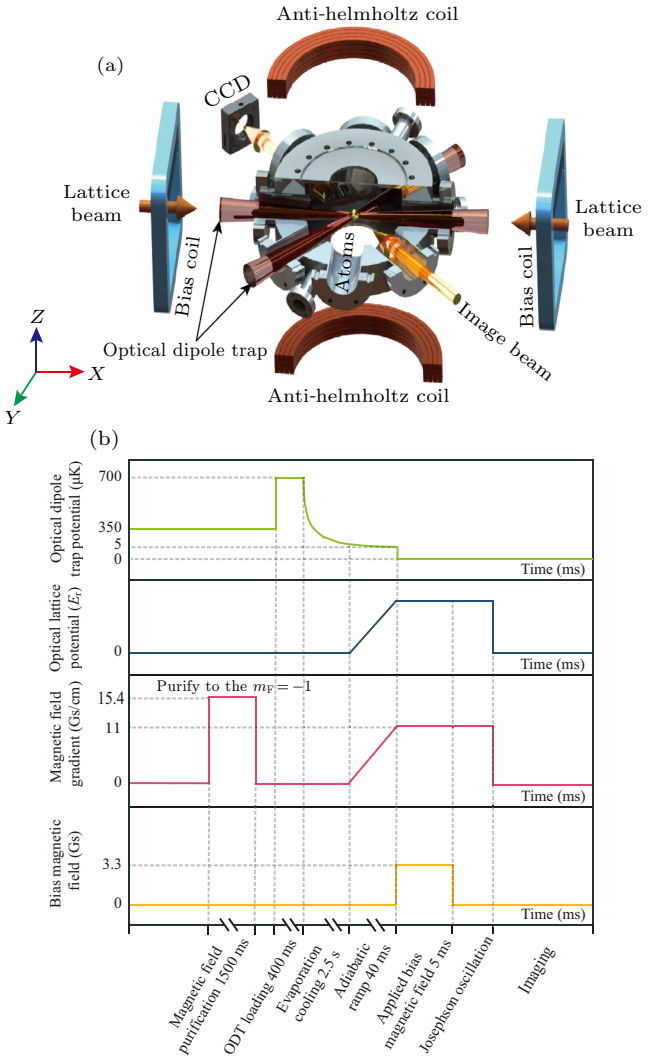


Fig. 1. Experimental scheme. (a) Sketch of experimental setup. A ^{23}Na BEC is prepared in an ODT formed by two 1064-nm laser beams with different $1/e^2$ radius. A 1D optical lattice is used to create a Josephson junction array in which atoms are induced to tunnel through the array by a combination of a bias magnetic field and a magnetic field gradient $\partial B/\partial z$. (b) Schematic diagram of experimental time sequence. Atoms are loaded into the dipole trap and cooled to form BEC via evaporation cooling. A gradient magnetic field is applied for 1500 ms to prepare the pure initial state $|F = 1, m_F = -1\rangle$. Subsequently, the atoms are transferred to the combined trap over a 40-ms ramp-up period. With a biased magnetic field, the atoms are confined in the combined trap for displacement measurement relative to the initial position with absorption imaging.

The experimental sequence is depicted in Fig. 1(b). Initially, the pure quantized state $|F = 1, m_F = -1\rangle$ is prepared using a magnetic field gradient of 15.4 Gs/cm (1 Gs = 10^{-4} T) prior to evaporative cooling.[45] The lattice beam is switched on by the AOM, whose voltage is ramped up from 0 to the final value. In parallel, the gradient field ramps up from zero to 11 Gs/cm. Both the magnetic field and the lattice are held for 40 ms to the final value in order to avoid significant atomic loss. After this stage, the atoms are transferred to a combined trap consisting of magnetic harmonic trap and an optical periodic potential. A constant current is applied to the bias coils,

leading to a magnetic field of 3.3 Gs aligned with the optical lattice axis. Following a 5-ms duration of the bias magnetic field, it is abruptly turned off while the atoms remain in the combined trap before the stage of time of flight with 6 ms. Finally, the displacement of the atoms relative to their initial position is detected by absorption imaging.

4. Results and discussion

With the application of a bias magnetic field, the null point of the magnetic field exhibits a slight displacement from its original position, and the coherent collective oscillations of atoms become distinctly observable. In Fig. 2, we show a coherent collective oscillation of atoms within the combined trap. First-order diffraction peaks at $\pm 2\pi\hbar/\lambda$ are observed in the momentum space following the regulation of the optical lattice. Atomic oscillation data have been fitted using the sinusoidal function $x = x_0 + A\sin[\omega(t - t_c)]$, where A denotes the amplitude and ω represents the angular frequency. The measured oscillation frequencies for the central momentum peak and the two first-order diffraction peaks are 113.65 Hz, 113.16 Hz, and 113.49 Hz, respectively. The nearly identical oscillation frequencies of these three diffraction peaks indicate a consistent quantum coherence throughout the oscillation process.

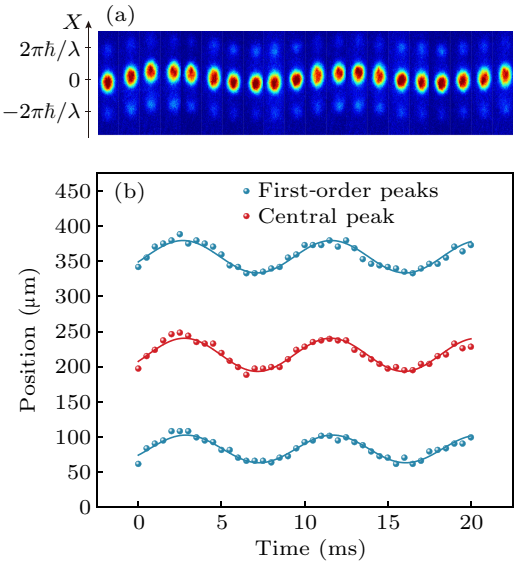


Fig. 2. (a) Depicts the coherent collective oscillations of the three momentum peaks in the combined trap. (b) The central positions of the three momentum peaks as a function of the time subsequent to a magnetic field displacement. The central peak is indicated by red spheres, whereas the first-order diffraction peaks are marked by blue spheres.

Figure 2 demonstrates the stable quantum coherence of atoms within a Josephson array, constructed by an optical lattice. Based on the global phase coherence condition, we observe the collective oscillatory motion of atoms following the application of the bias magnetic field. As a valuable indicator for monitoring the tunneling dynamics of the condensate in the potential well, we focus on the variations in the position of the central peak. Figure 3 presents a comparative analysis of atomic oscillation frequencies in the presence and absence of the lattice potential field. The axial and radial capture frequencies of the lattice are $\omega_x = 2\pi \times 12.7$ kHz and $\omega_r = 2\pi \times 78$ Hz, respectively. With a slight shift in the null point of the magnetic field, atoms exhibit oscillation both with or without the optical standing wave. We utilize the identical function as depicted in Fig. 2 to fit the data. In the presence of the lattice, the oscillation frequency is recorded as 147.16 Hz, while in its absence, the oscillation frequency measures 152.71 Hz. The superimposed optical lattice potential forms a periodic potential well, which inhibits the quantum tunneling of atoms and decrease the oscillation frequency as they traverse adjacent wells.

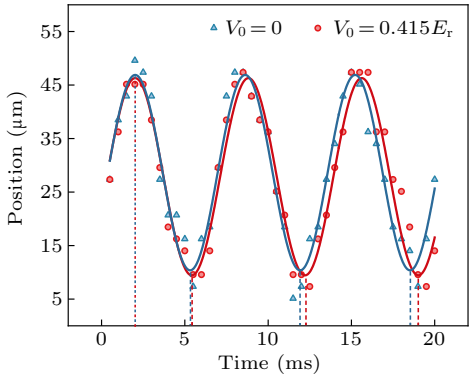


Fig. 3. The central position of the central peak as a function of time in the presence and absence of the lattice potential field. Atomic oscillation in the absence (presence) of a standing wave is represented by the blue triangles (red circles). The solid lines represent the sinusoidal fits to the data, and the dashed vertical lines indicate the frequency shifts associated with or without the optical standing wave.

Finally, we further measure the relationship between the Josephson oscillation frequency and the lattice potential depth. The depth can be precisely altered by manipulating the laser power. We scanned the energy V_0 from $1.07E_r$ to $2.49E_r$, which is much higher than the chemical potential of the condensate, with a step of $0.18E_r$. Figure 4 shows the measurement of the Josephson oscillation frequency as a function of the lattice depth. The square of the oscillation frequency is directly proportional to the microscopic tunneling rate of the condensate through the barriers. The red solid curve represents the quadratic fit to the data. As expected, the oscillation frequency exhibits a decreasing trend with increasing potential depth. From Eq. (8), we derive a direct expression for the critical current based on the Josephson oscillation frequency, which is associated with both the atomic oscillation frequency ω in the lattice and the atomic oscillation frequency ω_0 in the absence of a periodic potential field. In the Josephson junction, the Josephson critical current J_0 is directly proportional to the tunneling rate. This condition effectively restricts the maximum velocity of the condensate flow through the adjacent well, thereby reducing the oscillation frequency. Therefore, our experiment clearly demonstrates that the dynamics of Bose–Einstein condensates (BECs) within a lattice structure

are governed by a nonlinear Schrödinger equation. Furthermore, the Josephson effect has been successfully observed in ultracold atomic gases through a Josephson array.

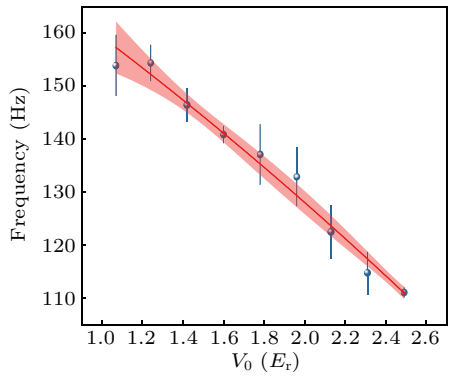


Fig. 4. Dependence of the Josephson oscillation frequency on the lattice depth. The experimental data, derived from sinusoidal fits to the oscillatory curves, is represented by blue spheres. The trend line is depicted by a quadratic fit to the data, with a 95% confidence interval (shown in red shading) that quantifies the uncertainty in the predicted frequency values.

5. Conclusion

The phenomenon of Josephson current is successfully observed in the ultracold sodium Bosonic gas system. With a precisely designed optical lattice system, we investigated the Josephson effect by driving the tunneling motion of atoms between adjacent wells using a bias magnetic field. This research demonstrates the applicability of the Josephson junction in ultracold Bosonic atomic systems and provides a firm experimental foundation for the study of Josephson junction dynamics.

Acknowledgements

Project supported by the Innovation Program for Quantum Science and Technology (Grant No. 2021ZD0302103), the National Natural Science Foundation of China (Grant Nos. 62325505, 62020106014, 62175140, 62475138, 92165106, and 12104276), and the Shanxi Province Graduate Student Research Innovation Project (Grant No. 2024KY105).

References

[1] Josephson B D 1962 *Phys. Lett.* **1** 251
[2] Anderson P W and Rowell J M 1963 *Phys. Rev. Lett.* **10** 230
[3] Avenel O and Varoquaux E 1988 *Phys. Rev. Lett.* **60** 416
[4] Pereverzev S V, Loshak A, Backhaus S, Davis J C and Packard R E 1997 *Nature* **388** 449
[5] Sukhatme K, Mukharsky Y, Chui T and Pearson D 2001 *Nature* **411** 280
[6] He K, Geng X, Huang R, Liu J and Chen W 2021 *Chin. Phys. B* **30** 080304
[7] Liu W Y, Zheng D N and Zhao S P 2018 *Chin. Phys. B* **27** 027401
[8] Wang B, Tan L, Lü C H and Tan W T 2010 *Chin. Phys. B* **19** 117402
[9] Betz T, Manz S, Bücker R, Berrada T, Koller C, Kazakov G, Mazets I E, Stimming H P, Perrin A, Schumm T and Schmiedmayer J 2011 *Phys. Rev. Lett.* **106** 020407
[10] Zapata I, Sols F and Leggett A J 1998 *Phys. Rev. A* **57** R28
[11] Raghavan S, Smerzi A, Fantoni S and Shenoy S R 1999 *Phys. Rev. A* **59** 620
[12] Williams J, Walser R, Cooper J, Cornell E and Holland M 1999 *Phys. Rev. A* **59** R31
[13] Zibold T, Nicklas E, Gross C and Oberthaler M K 2010 *Phys. Rev. Lett.* **105** 204101
[14] Hou J, Luo X W, Sun K, Bersano T, Gokhroo V, Mossman S, Engels P and Zhang C 2018 *Phys. Rev. Lett.* **120** 120401
[15] Valtolina G, Burchianti A, Amico A, Neri E, Xhani K, Seman J A, Trombettoni A, Smerzi A, Zaccanti M, Inguscio M and Roati G 2015 *Science* **350** 1505
[16] Albiez M, Gati R, Fölling J, Hunsmann S, Cristiani M and Oberthaler M K 2005 *Phys. Rev. Lett.* **95** 010402
[17] Gati R and Oberthaler M K 2007 *J. Phys. B: At. Mol. Opt. Phys.* **40** R61
[18] Levy S, Lahoud E, Shomroni I and Steinhauer J 2007 *Nature* **449** 579
[19] Ryu C, Blackburn P W, Blinova A A and Boshier M G 2013 *Phys. Rev. Lett.* **111** 205301
[20] Zou P and Dalfovo F 2014 *J. Low Temp. Phys.* **177** 240
[21] Pigneur M, Berrada T, Bonneau M, Schumm T, Demler E and Schmiedmayer J 2018 *Phys. Rev. Lett.* **120** 173601
[22] LeBlanc L J, Bardon A B, McKeever J, Extavour M H T, Jervis D, Thywissen J H, Piazza F and Smerzi A 2011 *Phys. Rev. Lett.* **106** 025302
[23] Spagnolli G, Semeghini G, Masi L, Ferioli G, Trenkwalder A, Coop S, Landini M, Pezzè L, Modugno G, Inguscio M, Smerzi A and Fattori M 2017 *Phys. Rev. Lett.* **118** 230403
[24] Wang P J, Fu Z K, Chai S J and Zhang J 2011 *Chin. Phys. B* **20** 103401
[25] Huang L H, Wang P J, Fu Z K and Zhang J 2011 *Chin. Phys. B* **23** 013402
[26] Wang Y F, Zhang J H, Li Y Q, Wu J Z, Liu W L, Mei F, Hu Y, Xiao L T, Ma J, Chin C and Jia S T 2022 *Phys. Rev. Lett.* **129** 103401
[27] Li Y Q, Zhang J H, Wang Y F, Du H Y, Wu J Z, Liu W L, Mei F, Ma J, Xiao L T and Jia S T 2022 *Light. Sci. Appl.* **11** 13
[28] Wang Y F, Du H Y, Li Y Q, Mei F, Hu Y, Xiao L T, Ma J and Jia S T 2023 *Light. Sci. Appl.* **12** 50
[29] Momme M R, Bidasyuk Y M and Weyrauch M 2019 *Phys. Rev. A* **100** 033601
[30] Spuntarelli A, Pieri P and Strinati G C 2007 *Phys. Rev. Lett.* **99** 040401
[31] Zaccanti M and Zwerger W 2019 *Phys. Rev. A* **100** 063601
[32] Luick N, Sobirey L, Bohlen M, Singh V P, Mathey L, Lompe T and Moritz H 2020 *Science* **369** 89
[33] Kwon W J, Del Pace G, Panza R, Inguscio M, Zwerger W, Zaccanti M, Scazza F and Roati G 2020 *Science* **369** 84
[34] Cataliotti F S, Burger S, Fort C, Maddaloni P, Minardi F, Trombettoni A, Smerzi A and Inguscio M 2001 *Science* **293** 843
[35] Ramanathan A, Wright K C, Muniz S R, Zelan M, Hill III W T, Lobb C J, Helmerson K, Phillips W D and Campbell G K 2011 *Phys. Rev. Lett.* **106** 130401
[36] Dalfovo F, Giorgini S, Pitaevskii L P and Stringari S 1999 *Rev. Mod. Phys.* **71** 463
[37] Trombettoni A and Smerzi A 2001 *Phys. Rev. Lett.* **86** 2353
[38] Feynman R P, Leighton R B and Sands M 2010 (1965) *The Feynman Lectures on Physics* (Basic Books: California Institute of Technology) Vol. III, Chap. 21
[39] Dahan M B, Peik E, Reichel J, Castin Y and Salomon C 1996 *Phys. Rev. Lett.* **76** 4508
[40] Burger S, Cataliotti F S, Fort C, Minardi F, Inguscio M, Chiofalo M L and Tosi M P 2001 *Phys. Rev. Lett.* **86** 4447
[41] Liu W L, Zheng N X, Sovkov V, Xu J, Li Y Q, Fu Y M, Li P, Wu J Z, Ma J, Xiao L T and Jia S T 2022 *Phys. Chem. Chem. Phys.* **24** 15135
[42] Zheng N X, Liu W L, Sovkov V B, Xu J, Ge G Y, Li Y Q, Li P, Fu Y M, Wu J Z, Ma J, Xiao L T and Jia S T 2021 *Opt. Express* **29** 32892
[43] Liu W L, Zheng N X, Wang X F, Xu J, Li Y Q, Sovkov V B, Li P, Fu Y M, Wu J Z, Ma J, Xiao L T and Jia S T 2021 *J. Phys. B: At. Mol. Opt. Phys.* **54** 155501
[44] Liu W L, Zheng N X, Jian J, Tian L, Wu J Z, Li Y Q, Fu Y M, Li P, Sovkov V, Ma J, Xiao L T and Jia S T 2022 *Chin. Phys. B* **31** 073702
[45] Black A T, Gomez E, Turner L D, Jung S and Lett P D 2007 *Phys. Rev. Lett.* **99** 070403